Smart Structures and Systems, *Vol. 21, No. 5 (2018) 623-635*
DOI: https://doi.org/10.12989/sss.2018.21.5.623

Study on mechanical behaviors of large diameter shield tunnel during assembling

Kun Feng[1], Zuzhao Peng[1], Chuang Wang[1], Chuan He*[1], Qianshen Wang[1], Wei Wang[1], Songyu Cao[1], Shimin Wang**[1] and Haihua Zhang[2]

[1]Key Laboratory of Transportation Tunnel Engineering, Ministry of Education, Southwest Jiaotong University, Chengdu 610031, China
[2]Technical Research & Development Institute, Kumagai Gumi Co., Ltd, Ibaraki 300-2651, Japan

(Received December 12, 2017, Revised March 27, 2018, Accepted March 31, 2018)

Abstract. In order to study the mechanical behavior of shield tunnel segments during assembly stage, the in-situ tests and FDM numerical simulation were conducted based on the Foguan Shiziyang Tunnel with large cross-section. Analysis for the load state of the assembling segments in different assembly steps as well as the investigation for the changing of inner forces and longitudinal stress of segments with assembling steps were carried out in this paper. By comparing the tested results with the simulated results, the conclusions and suggestions could be drawn as follows: (1) It is the most significant for the effects on axial force and bending moment caused by the assembly of adjacent segment, followed by the insertion of key segment while the effects in the other assembly steps are relative smaller. With the increasing value of axial force, the negative bending moment turns into positive and remains increasing in most monitored sections, while the bending moment of segment B1and B6 are negative and keeping increasing; (2) The closer the monitored section to the adjacent segments or the key segment, the more significant the internal forces response, and the monitored effects of key segment insertion are more obvious than that of calculation; (3) The axial forces are all in compression during assembling and the monitored values are about 1.5~1.75 times larger than the calculated values, and the monitored values of bending moment are about 2 times the numerical calculation. The bending moment is more sensitive to the segments assembly process compared with axial force, and it will result in the large bending moment of segments during assembling when the construction parameters are not suitable or the assembly error is too large. However, the internal forces in assembly stage are less than those in normal service stage; (4) The distribution of longitudinal stress has strong influence on the changing of the internal forces. The segment side surface and intrados in the middle of two adjacent jacks are the crack-sensitive positions in the early assembly stage, and subsequently segment corners far away from the jacks become the crack-sensitive parts either.

Keywords: shield tunnel; assembling segments; mechanical behavior; in-situ tests; FDM numerical simulation

1. Introduction

Nowadays, segmental linings, the main structure of shield tunnel has been widely used in construction of metro tunnels and underwater tunnels. However, the breakages are easily induced in large volume RC segments particularly in manufacturing, transporting and assembling. It's verified by lots of tunneling projects that the stress state of segmental linings are complex due to its randomness and uncertainty, and with the increasing cross-section of shield tunnels, the breakages in assembly stage are often caused by the factors including segments assembling and grouting, etc., which have become more unfavorable for structure safety of shield tunnels. As the development of tunnel segments tends to be large-section structure and to be subject to high water and soil loads, etc. (Feng *et al*. 2013), as a result, temporal and spatial distribution laws of segmental linings are becoming more concerning during assembly stage.

In the late 1990s, Blom established a three-dimensional finite element model to study the mechanical characteristics of segment structure of the Heinenoord tunnel in assembling stage and inhomogeneous distributions have been observed for the stress of segment structure in assembly stage and the values of axial force in assembling stage reaches more than 60% of those in normal service stage (Blom *et al*. 1999). In the early 2000s, an analytic model for segment structure in assembly stage was established by Japanese scholars (Ishimura *et al*. 2003), part of segment self-weight was taken into account in the model, moreover, the analysis results have been compared with monitored values in in-situ tests. Wu has found that segment breakages in assembling stage accounts for 38.2% of that in the life cycle of a shield tunnel via the investigation of Shanghai metro tunnel (Wu *et al.* 2004). Sugimoto adopted the statistical method to analyze the reasons and classification of segments breakages in assembling stage and has put forward the corresponding control strategies for tunnel construction (Sugimoto *et al*. 2006). A three dimensional finite model was established by Chen and Mo to analyze the mechanical behaviors of segments in construction stage, furthermore, sensitivity analysis were carried out on the impacts of jack thrust and adjustment of

∗Corresponding authors, Ph.D.
E-mail: chuanhe21@swjtu.edu.cn
** E-mail: neumining@163.com

http://www.techno-press.com/journals/sss&subpage=7 ISSN: 1738-1584 (Print), 1738-1991 (Online)

shield attitude as well as assembly error. They had also indicated the breakage-sensitive parts of segments in assembly stage and suggested the corresponding precautions (Chen and Mo, 2008, Mo *et al*. 2009, Mo and Chen 2009). Cavalaro *et al.* established a three dimensional FEM model for assembly stage to study the crack problems resulted from contact deficiencies, besides, the influence of structural stiffness as well as segment's width and thickness were analyzed subsequently (Cavalaro *et al.* 2011, Cavalaro *et al.* 2012). In recent years, a segment structural analytic model was established by ignoring segment weight and size difference, and the analytic results were compared with the field monitored data of Qianjiang tunnel by Liao, et al. They found that the monitored values of internal force in assembling stage are about 30% of that in normal service stage but obviously greater than the analytic values (Liao *et al*. 2013, Liao *et al*. 2015).

The existing studies indicate that segmental structure in assembly stage will produce different mechanical responses, which could possibly lead to breakages on segments. Obviously, the analysis is significant for the mechanical characteristics of segments during assembling, of which guidance can be concluded for rational design and construction for shield tunnels. Nevertheless, the monitored data of in-situ tests are rarely recorded due to its high cost and great difficulty. As for the analytic model, it is debatable for the practicability and the rationality of basic hypothesis and mostly the impacts of jack thrust are ignored. When it comes to numerical simulation, most of the existing researches focus on the influence of construction parameters on segments in the ring erection process of whole or local segments. However, only a few studies have been carried out for three-dimensional model influenced by assembly steps and assembly method (symmetrical or asymmetric assembly). On the purpose of better acknowledgement for the mechanical characteristic of segments in assembling, analysis of constructing loads is conducted in assembly stage at first and subsequently a three-dimensional finite difference method (FDM) model is established in this paper based on Foguan Shiziyang Tunnel in which a segment ring covered with typical strata is presented for the in-situ tests. Furthermore, comparison of the numerical results and the monitored results is carried out to reveal the mechanical response on segment structure during assembling.

2. Load analysis in assembly stage

During assembly processes, segments locating at shield tail are subject to complex constructing loads including jack thrusts, grease pressure, bolt preload, segment self-weight and interaction force between structures (segment and segment, segment and tail brushes) as well as assembling forces caused by contact deficiencies and assembling errors. Meanwhile, water and soil loads outside shield shell are mainly acted indirectly via grease pressure. For the segments in assembling process, however, grease pressure is negligible due to the sealing effect of tail brushes, which results in pressure transmission failure from outside the shield shell to the assembling ring.

Jack thrust is the main load on the assembling segments, and it could result in a large contact pressure between the assembling ring and the previous ring, which might bring a greater longitudinal compression deformation of the assembling segments when pre-tightening force of longitudinal bolts become relaxed as the value of jack thrust increases to a certain level. Therefore, pre-tightening force of longitudinal bolts are insignificant during segments assembling, in addition, according to the Saint-Venant's principle, it can be ignored for the influenced area of pre-tightening force in circumferential bolts due to the small value of the area compared with that of segments, thus, it is negligible in assembly stage as well.

When bolt pre-tightening force is ignored, self-weight and jack thrusts of the assembling segments are mainly balanced by segment contact pressure and friction forces in assembly stage, it can be explained as followed: on one hand, the shell's inner diameter is slightly larger than the segment's outer diameter, and thus segments of the assembling ring could not be contacted with shield shell directly due to shield tail gap. On the other hand, because of the certain clearance between the bolts hole and the bolts (Xu, 2013), the shear force in connecting bolts will be too small to make any difference on the balance of the assembling ring when a tiny assembly error occurred in certain circumstance. Therefore, as for the factors with strong randomness such as contact deficiencies and assembly errors, they are not taken into account in this paper.

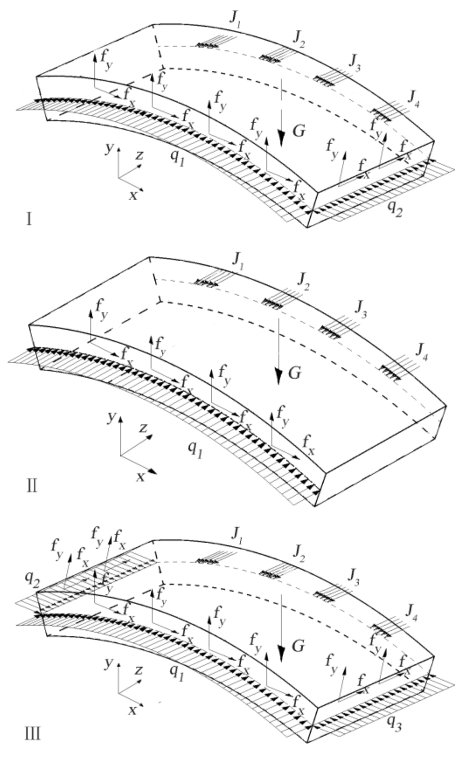

Fig. 1 Three types of segment mechanical mode in assembly stage

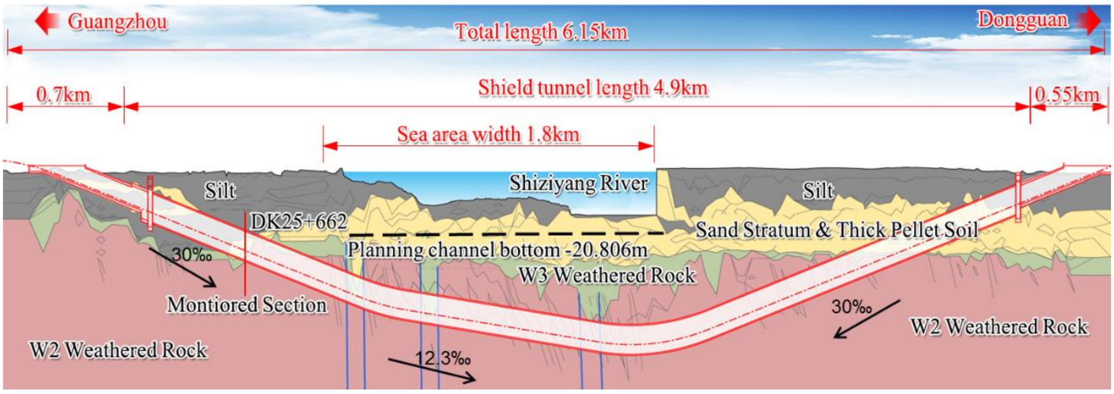

Fig. 2 Longitudinal profile of Foguan Shiziyang Tunnel

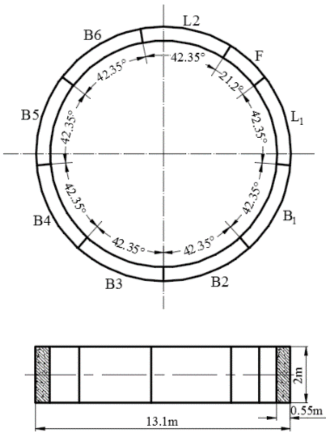

Fig. 3 Cross section of the segment structure

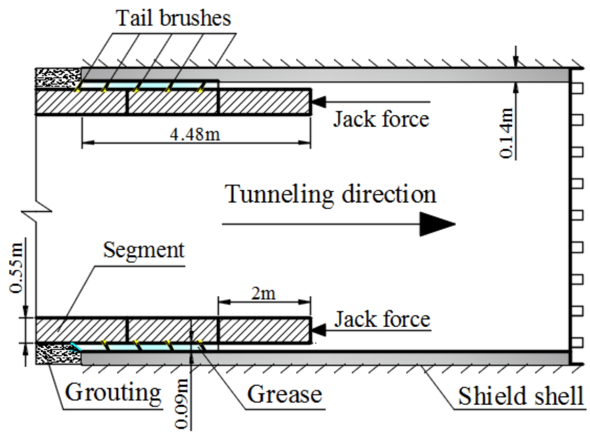

Fig. 4 Basic parameters of segments and shield tail

The assembling segments can be divided into three types in accordance with constraint conditions or contact conditions: (I) segments with no constraints on both sides, (II) segments with constraints on single side, (III) segments with constraints on both sides. To summarize, the three types of segment mechanical mode in assembly stage could be diagrammed as Fig. 1, where f_x, f_y, f_z are friction forces, J_1, J_2, J_3, are jack thrusts, q_1, q_2, q_3, are segmental contact pressures, G is segment weight.

3. Scheme of in-situ test and numerical simulation

3.1 Project overview

Foguan Shiziyang Tunnel is an intercity railway tunnel with a total length of 6150 m and the crossing-river length of 1800 m. It crosses through quaternary marine sedimentary strata (including silt, sand and soil strata), and passed the full-face weathered rock (W3, W2) beneath the Pearl River in Guangzhou, with abundant and high underground water (the highest water pressure is about 0.67 MPa), the tunnel profile is shown in Fig. 2. The slurry balance shield method is applied for the tunnel construction and the cross-section of segmental lining is shown in Fig. 3, in which the lining ring is diagrammed and divided into nine blocks via the “1+2+6” block mode with outer diameter of 13.1 m and width of 2 m as well as thickness of 0.55 m. In addition, the universal wedge-shaped segments is adopted with 30 mm double-wedge is adopted and the segment ring is planned to build in staggered assembling. Joints are all connected with oblique bolts and 34 M36 bolts are arranged in the ring joints and 27 M36 bolts are placed in the longitudinal joints respectively. Besides, thickness of the shield shell is 0.14 m and width of the tail gap is 0.09 m, the shield tail is 4.88 m long with five tail brushes contacting with the last two segmental rings in the shield tail. Fig. 4 shows relative position between segments and shield shell in the shield tail.

3.2 Scheme of in-situ tests

In-situ test is widely adopted in many practical projects (Ye *et al.* 2013, Ye *et al.* 2018). The monitored ring locates at DK25+662, with upper-soft and lower-hard strata. Under the protection of the shied shell and tail brushes, as a result, water and ground load and ground condition become the negligible factors. As shown in Fig. 5, the monitored ring is assembled in an asymmetric order of B3-B2-B1-L1-B4-B5-B6-L2-F. The specific assembly process is described as follows: first of all, segment B3 is moved to the design position by the segments installation machine after the retraction of corresponding jack cylinders. Subsequently, when segment B3 becomes stable, jack thrusts are applied on segment B3 with the extension of jack cylinders and then longitudinal bolts are installed in the corresponding hand holes. Afterwards, segment B2~ segment L2 are assembled in the similar way, however the difference is: while the longitudinal bolts will be installed after the stabilization of each segment assembly for both type of segments, the circumferential bolts should be installed for B2~L2 segments. Proverbially, the insertion of key segment is the critical step of assembling, in the first place, the key segment is moved to the vicinity of the design position by the segments installation machine, meanwhile, it does not contact with the adjacent segments but located at the 2/3 of the longitudinal design position in that case. Then, with the uplifting of the segments installation machine, the key segment is inserted along the radial direction and subsequently it's pushed into the design position along the longitudinal direction by jack thrusts. Finally, both the longitudinal bolts and the ring bolts are installed for key segment, and the whole segmental ring was accomplished.

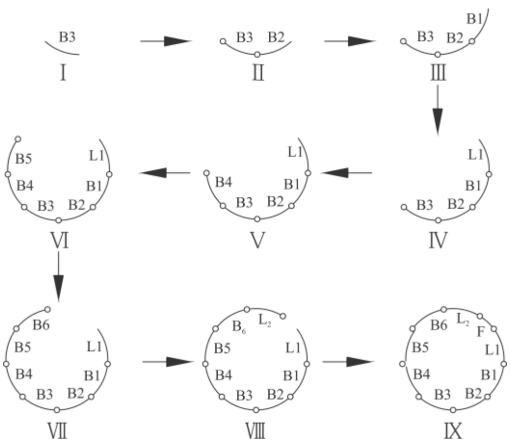

Fig.5 Assembly steps of the monitored ring

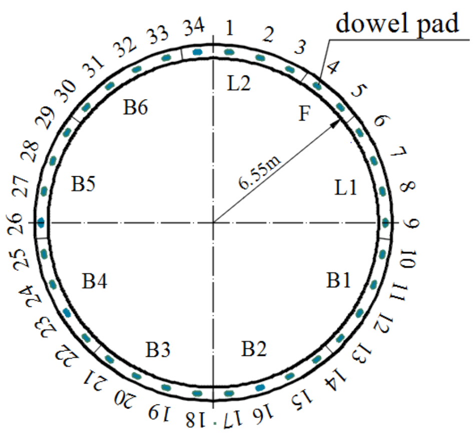

Fig.6 Position of dowel pads

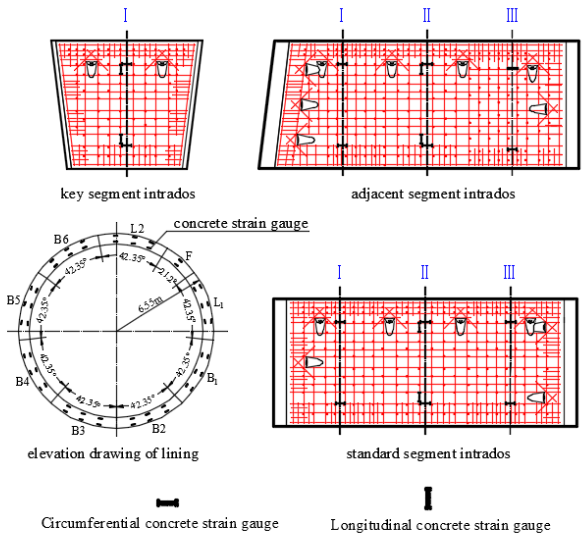

Fig. 7 Layout of sensors in the monitored ring

Furthermore, the assembly point of the monitored ring is planned according to the longitudinal alignment design. Taking the monitored ring presented in Fig. 6 for example, the assembling points are marked with dowel pads, and each point means a pair of jack thrusts is provided by jack cylinders via a dowel pad. In order to analyze mechanical characteristics of the assembling segments, 136 vibrating concrete strain gauges are embedded in the monitored segments to investigate the temporal-spatial distribution of axial force and bending moment as well as the strain and stress of the assembling ring. The strain gauges are tied on steels and arranged closely to segment intrados and extrados. The layout of the gauging points is diagramed as Fig. 7, in which, three monitored sections of internal force are applied for adjacent block and standard block in ring direction while only one monitored section is selected for key segment, however, the monitored sections of the longitudinal stress is placed for every segment. For those segments, the monitored sections of internal forces in ring direction are arranged between the adjacent jack cylinders, of which the central angles between those monitored sections are 10.588°, besides, the monitored sections for the longitudinal stress are chosen in the middle of the segments. During the assembly stage, the data of the strain gauges in all assembled segments of the assembling ring are collected manually as soon as the completion of each assembly step.

3.3 Scheme of numerical calculation

Obviously, it is difficult to deduce the analytic stress and strain solutions of segments in under the complex force and displacement boundaries during assembling. It's rational to use numerical methods to solve this issue. Compared with the finite element method (FEM), the finite difference method (FDM) has advantages in fast convergence rate and low complexity as well as mature theory and application, moreover, discretization error of FDM is easy to be lower than that of FEM (Oliveira and Chen 1985). Therefore, as shown in Fig. 8, a numerical model is established via

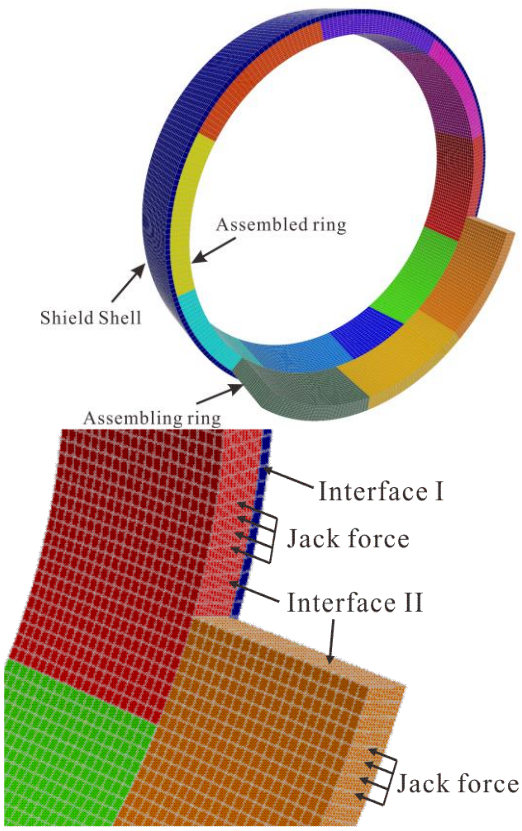

Fig. 8 Finite difference model of segmental ring during assembling

ANSYS pre-processing module and calculated in the FDM software FLAC^{3D} to simulate the assembly process of Foguan Shiziyang Tunnel. The element type in ANSYS pre-processing module are all Soild45. When it's imported to FLAC^{3D}, all the elements of shield shell and segments turn into brick element, what's more, the structural element interface was applied to simulate the contact relation of the numerical model during FDM calculation. The geometry size of the numerical model is defined according to Figs. 3 and 4, and the algorithms of numerical simulation during segments assembling is conducted as the followings:

Step 1: firstly, the initial element grid model is imported to FLAC^{3D} and horizontal, vertical and longitudinal displacement constraints are imposed on extrados surface of the shield shell while only the longitudinal displacement constraints are imposed at the head surface along the width direction of the assembled ring which is far away from the jacks.

Step 2: segments of the assembling ring are 'deleted' by and then jack thrusts are applied on the assembled ring. The interface elements of interface I are imposed on the contact surfaces between the shield shell and the assembled ring to simulate the interaction between tail brushes and segments. Afterwards the initial calculation is activated.

Step 3: in each assembly step, jack thrusts applied on the assembled ring at the corresponding points are removed to simulate retraction of the jacks.

Step 4: the elements of the assembling segment in current step are activated and then the interface elements of interface II are imposed on the contact surfaces among the segments to simulate their interaction.

Step 5: the jack thrusts are applied on the current assembling segment at the corresponding points to simulate the restraining effect of the jacks on the current assembling segment.

Step 6: loop is accomplished for step 3 to step 5 until the last assembly step, in which the whole assembly process of the assembling ring can be obtained.

The hexahedron elements are adopted to simulate the segments while interface elements with different properties are adopted to simulate the interaction among segments as well as segment and tail brushes. The normal stiffness and tangential stiffness of the interface elements are calculated by the formula 1 (Itasca Consulting Group, 2005), where k_n and k_s are the normal stiffness and tangential stiffness respectively; and K is the bulk moduli while G_s is the shear moduli; $\Delta z_{\min}$ is the smallest width of an adjoining zone in the normal direction.

$$k_n = k_s = 10\max\left[\frac{K+\frac{4}{3}G_s}{\Delta z_{\min}}\right] \tag{1}$$

Guo *et al.* and Feng *et al.* proposed that static friction coefficient of concrete contact surface is around 0.5~0.57 through the segment joint test and Zhao, et al. suggested that static friction coefficient is about 0.5~0.7 through the contact surface test of RC segment. Hence according to Guo, Feng and Zhao's study, the static friction coefficient of concrete contact surface between the segments is around 0.5~0.57 (Guo *et al.* 2011, Zhao *et al.* 2015, Feng *et al.* 2018), so the static friction coefficient of this FDM model is set to be 0.5 for the interface I, while it is set as 0.3 for the interface II, and cohesion of all interfaces is set as 0 (Mo and Chen, 2008). In addition, the total thrust of the jacks is 60,000 kN and it is averagely distributed to 34 pairs of jacks. The thrust of each jack is also evenly distributed to the nodes that in the range of the jack boots so as to conduct the application of the jack thrust. The relevant parameters used in the numerical model are listed in Table 1.

Table 1 The relevant parameter used in numerical model

Properties	Parameters
Segment	$E = 34.5\text{GPa}, \upsilon = 0.2, \gamma = 25\text{kN}\cdot\text{m}^{-3}$
Shield	$E = 206\text{GPa}, \upsilon = 0.2, \gamma = 75\text{kN}\cdot\text{m}^{-3}$
Interface I	$k_n = k_s = 4.58\times10^4\text{GPa}, c = 0, \varphi = 16.7°$
Interface II	$k_n = k_s = 7667\text{GPa}, c = 0, \varphi = 25.56°$
Total jack thrust	$6\times10^4\,\text{kN}$
Number of jack cylinder	34

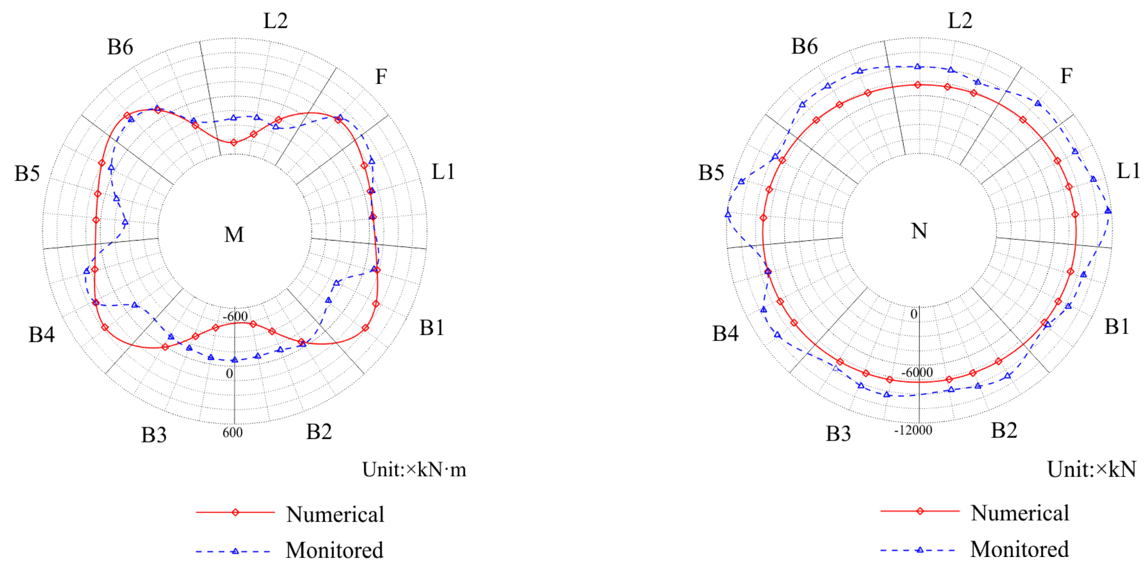

Fig. 9 Distribution of inner forces in normal service stage

4. Result analysis of in-situ test and numerical simulation

The analyses are conducted for temporal-spatial distribution laws of axial force and bending moment, as well as longitudinal stress and principle tensile stress of the assembling ring in depth by means of in-situ tests and numerical simulation to reveal the mechanism of segmental rings during assembling. Characteristics are shown as Fig. 9 for bending moment and axial force calculated by the beam-spring model of the monitored ring in normal service stage.

4.1 Changing of axial force during assembling

Time-history curves of axial force in segments of the assembling ring during the assembly stage are shown in Fig. 10. It is indicated that the calculation value of the monitored sections for axial force are all in state of compression within the range of -500 kN~-1600 kN while the effects of the stochastic factors are not taken into account such as assembly error, etc. The monitored results also implied that the sections are in state of compression, but due to the factors including assembly error and construction operation as well as contact deficiencies and adjustment of jack thrust, etc., all of the monitored values are about 1.5~1.75 times larger than the calculated values and within the range of -750 kN~-2800 kN. However, the axial forces are about 9.7%~33.9% of those in normal service stage.

As is shown in the numerical calculation results, for an assembled segment of the assembling ring, the corresponding effects vary from different assembly steps, of which effects caused by the assembly of adjacent segment are the most significant, followed by the insertion of key segment while effects of the other assembly steps are relative smaller. Moreover, the axial force of the assembled segment increases when it comes to the assembly of adjacent segment and the insertion of key segment. Furthermore, the closer the monitored section to the adjacent segment or key segment, the more significant the axial force responses. Influenced by the stochastic factors, fluctuation of the monitored value is larger than that of the numerical simulation, but the changes of axial force are generally in good consistency. It is remarkable that the monitored effects of key segment insertion are more obvious than that of the calculated value.

Fig. 11 shows the distribution of axial force in each assembly step, in which the overall distribution of axial force calculated by the FDM model is more uniform than the monitored value. Furthermore, since the arc length of segment extrados is larger than that of segment intrados, the restraining effects on both sides of a segment caused by the adjacent segments is more significant when the intrados of the segment is pointed to the gravity direction, consequently it results in a relative large normal contact pressure between segments and hence leads to the larger axial force of segments in the upper half ring compared with those in the lower half ring.

4.2 Changing of bending moment during assembling

Time-history curves of bending moment in segments of the assembling ring in the assembly stage are shown as Fig. 12. Mostly, the monitored sections are subject to positive bending moment which results in the compressed intrados and the tensile extrados of the segments, besides the calculated values are within -95.03 kN·m~69.4 kN·m. In the early assembly stage, most monitored sections bear negative bending moment and subsequently the restraining effect on both sides of a segment is becoming more significant along with the assembly steps, in which the negative bending moment is turned into the increasing positive bending moment in most monitored sections. For segment B1 and segment B6, however, the bending moments of them are both negative and decreasing. Similar to the behaviors of axial force, the assembly of adjacent segment causes the

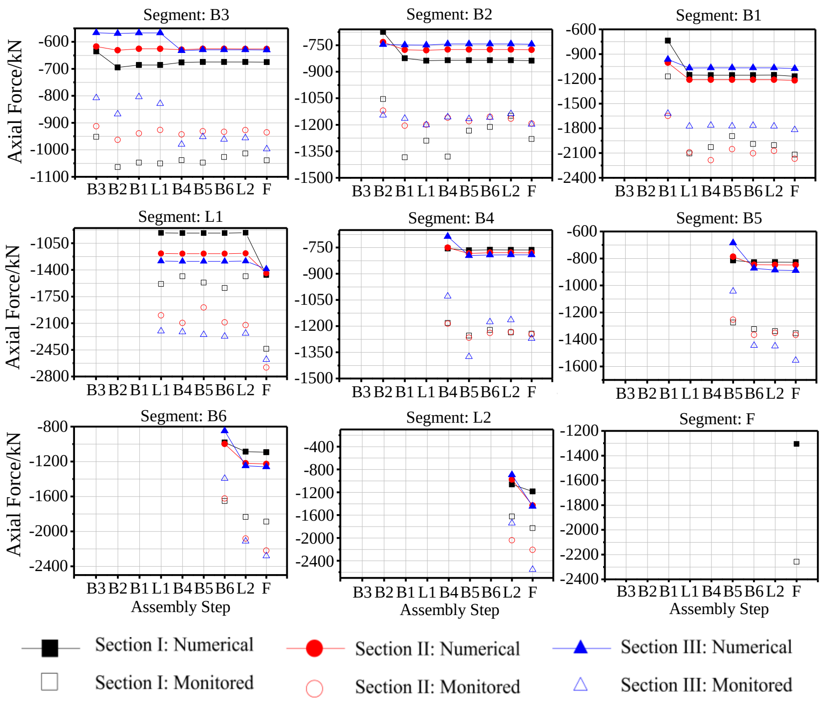

Fig. 10 Time history curves of axial force in assembly stage

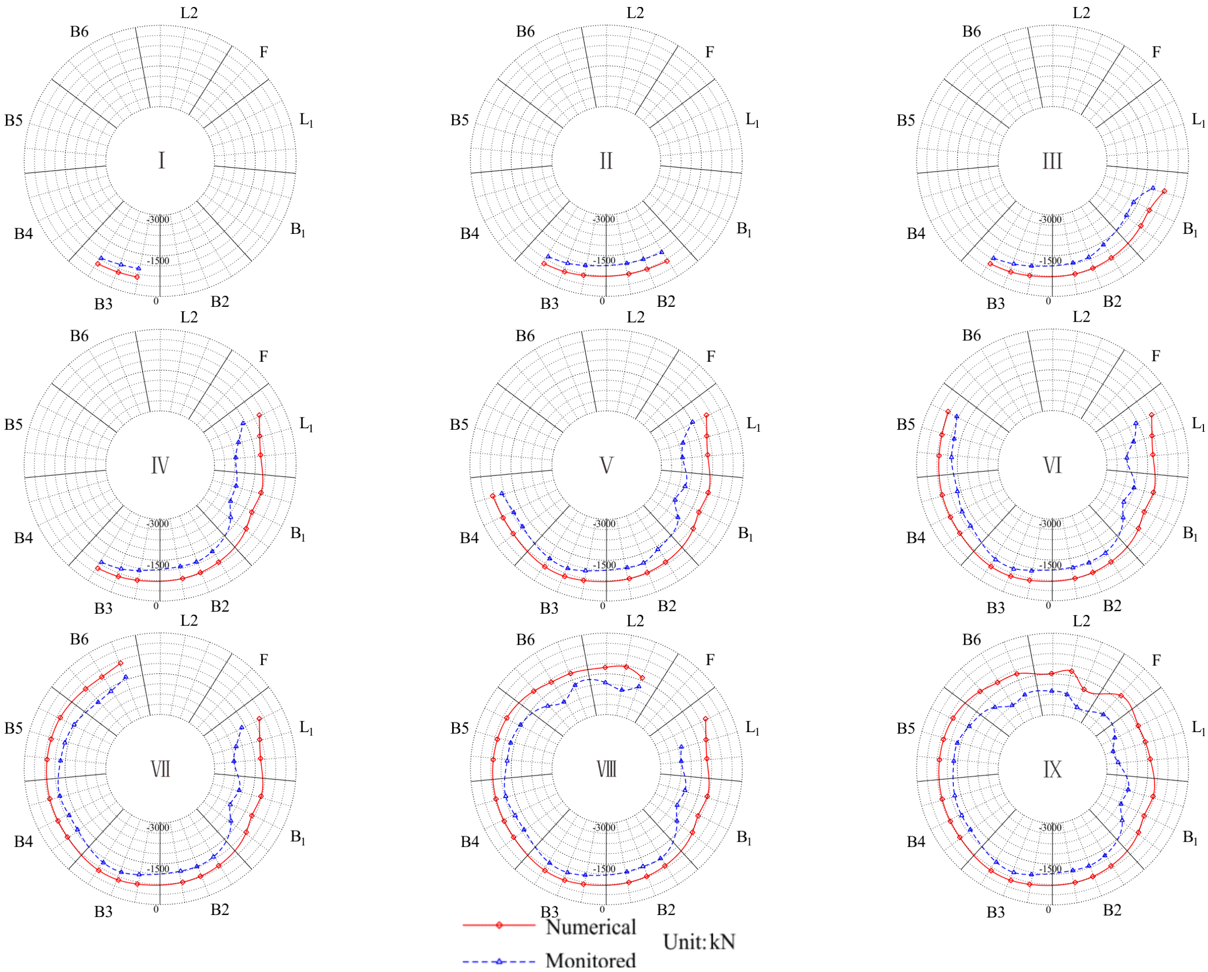

Fig. 11 The distribution of axial force in assembling

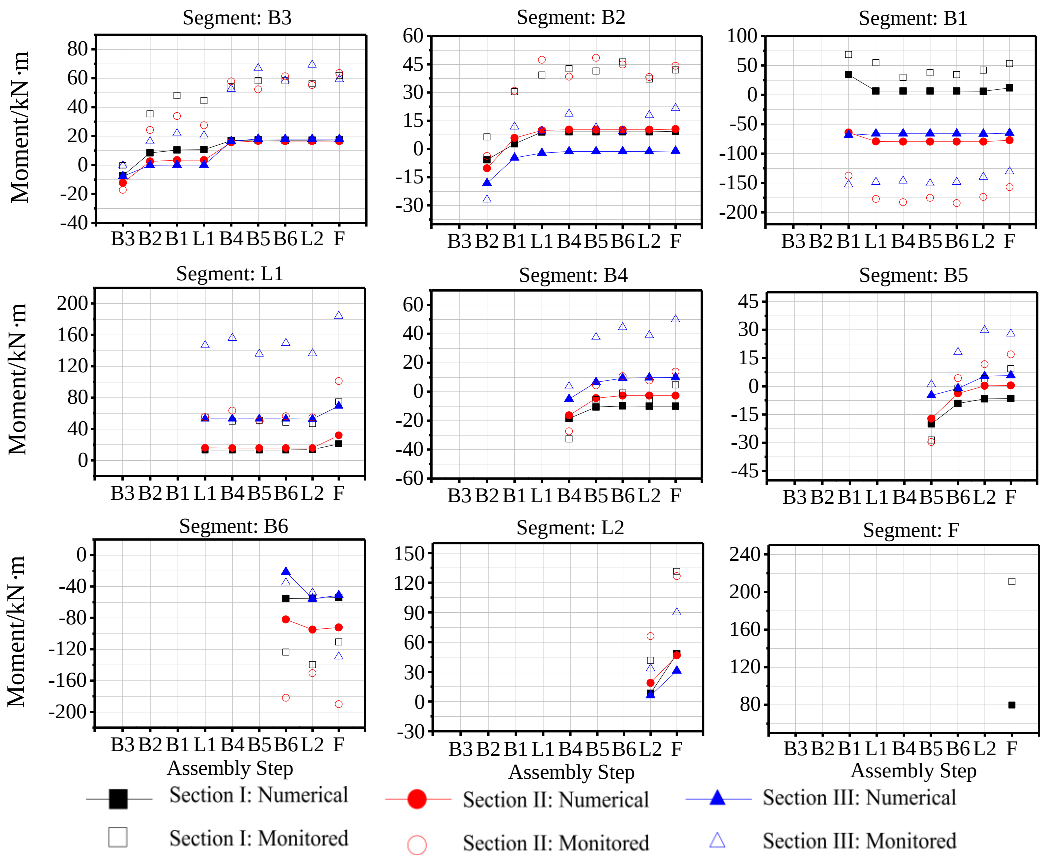

Fig. 12 Time history curves of bending moment in assembly stage

most significant changing, then followed by the insertion of the key segment, while the effects of the other assembly steps are relative smaller. The monitored values of bending moment during assembling are within -190.2 kN·m~211.1 kN·m, which are 2 times larger than the calculated values. The maximum values of the monitored positive bending moment and the negative bending moment during the assembly stage are about 59.4% and 39.3% of those in the normal service stage respectively. The changings of bending moment is more sensitive to the assembly process compared with axial force, and it will result in the large extra bending moment of segments during assembling if the construction parameters are not suitable or the assembly error is too large. As a result, it should be concerned in large cross-section shield tunnel assembling. Fig. 13 shows the distribution of bending moment in each assembly step and it indicates that the bending moment of the assembly segmental ring is almost symmetrically distributed along with middle line of the key segment after the segmental ring is erected in whole. Meanwhile, the segment B1 and the segment B6 are subject to large negative bending moment, while there are large positive bending moment in the segment L1 and the segment L2 as well as the segment B3. In addition, the bending moment of the other segments are relatively smaller.

4.3 Changing of longitudinal stress during assembling

The longitudinal stress is the main factor which causes axial force and bending moment response on the assembling segmental ring during assembly stage. To figure out how it works as well as its spatial distribution, sections are arranged in the middle of each segment to monitor the longitudinal stress in the monitored segmental ring. For each longitudinal stress monitored section, a pair of concrete strain gauges is arranged near the side surface close to the jacks (side A) and the side surface away from the jacks (side B) respectively. The mean value of longitudinal stress at intrados and extrados on the side A or the side B is adopted based on the plane section assumption. Succinctly, it is symbolized as or and the time history curves of and are shown in Fig. 14.

Moreover, it is indicated in the numerical results that the longitudinal stress of the monitored sections are all in compression with the value from -2.802MPa to -4.451MPa and the monitored values that within -4.012MPa~-11.979MPa are larger than the calculated value. Furthermore, the maximum increment value of the longitudinal stress in the numerical calculation is 87.6kPa while it is 738kPa in the in-situ tests.

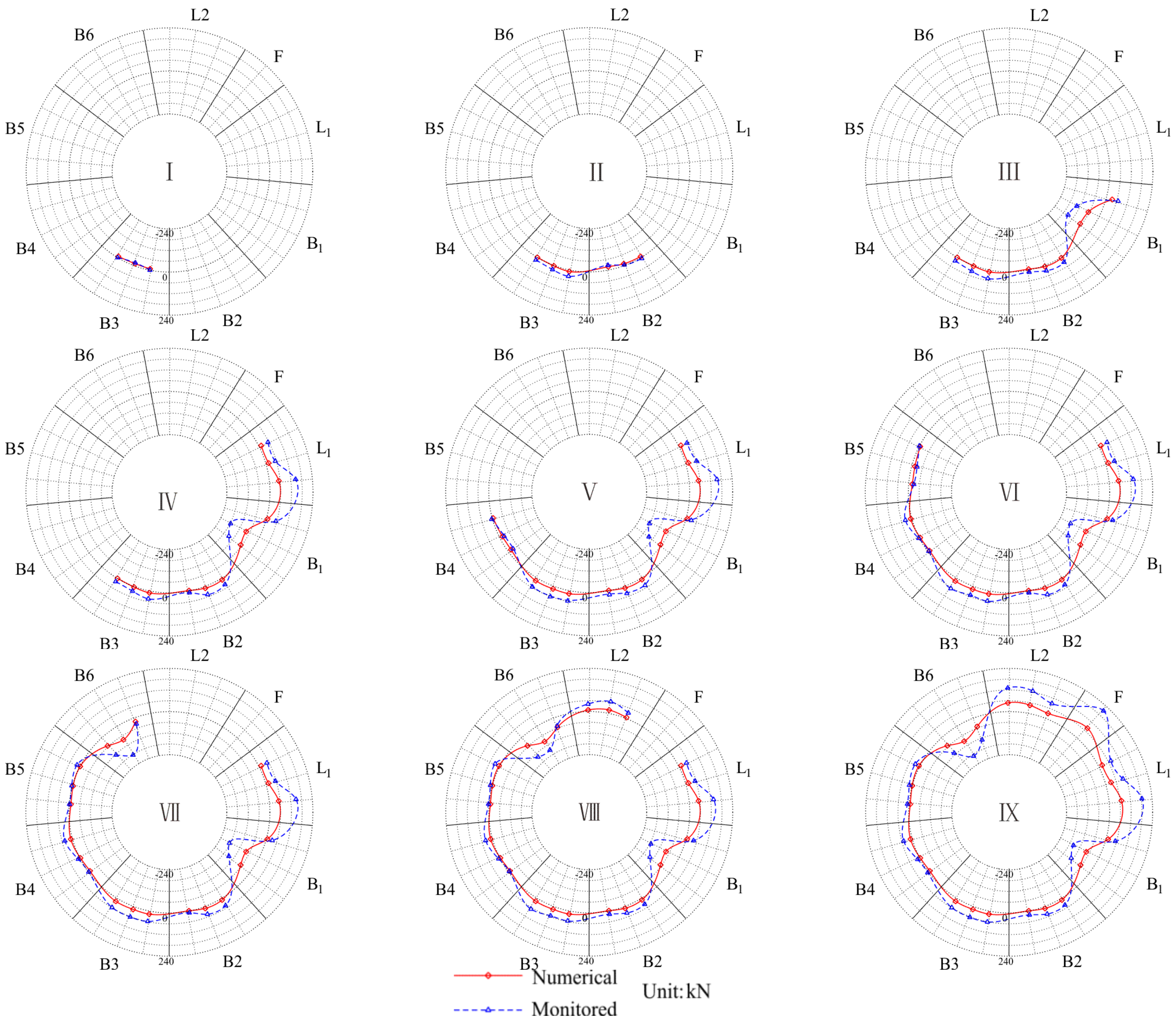

Fig. 13 The distribution of axial force in assembling

Although the disturbance of monitored results are greater than the calculation ones, there are still similarities in terms of their temporal-spatial distribution laws which is embodied by the following points: (1) the assembly of the adjacent segments and the insertion of key segment will result in the increment of longitudinal stress and the disturbance is greater than the other assembly steps; (2) is smaller than which means longitudinal stress of the side surface close to the jacks is smaller than that away from the jacks.

The first above-mentioned commonness shows the same law as the changing of axial force and bending moment, which indicates that the spatial distribution of segment longitudinal stress is the original factor causing the changing of inner forces during assembling. Fig. 15 shows the distribution of longitudinal stress of segment B3 after the ling ring is assembled in whole, besides it is indicated in the figure that the longitudinal stress increases at first and then decreases from side surface A to side surface B. Moreover, there is a local longitudinal tensile stress zone on segment side surface in the middle of two adjacent jacks on side surface A, and the segment is subject to longitudinal compression stress out of the zone. In fact, for each segment of the assembly ring, the presented law is embodied in each assembly stage, and hence the local tensile stress zone near the side surface A results in the second above-mentioned commonness.

4.4 Analysis of principle tensile stress of assembling segments

Fig. 16 shows the cracks occurred during assembly stage of Foguan Shiziyang Tunnel and according to the in-situ investigation, it could be summarized that the segment cracks in assembly stage usually appear in the following positions: 1) the side surface and the intrados in the middle of two adjacent jacks; 2) the intrados near the jacks; 3) the segment corners away from the jacks. The analysis of segment principal tensile stress is carried out to ascertain how the cracking occurred during assembling. The spatial distribution of the principal tensile stress of the assembly segments are shown in Figs. 17 and 18 for simulated assembly steps 1,2,5 and 9.

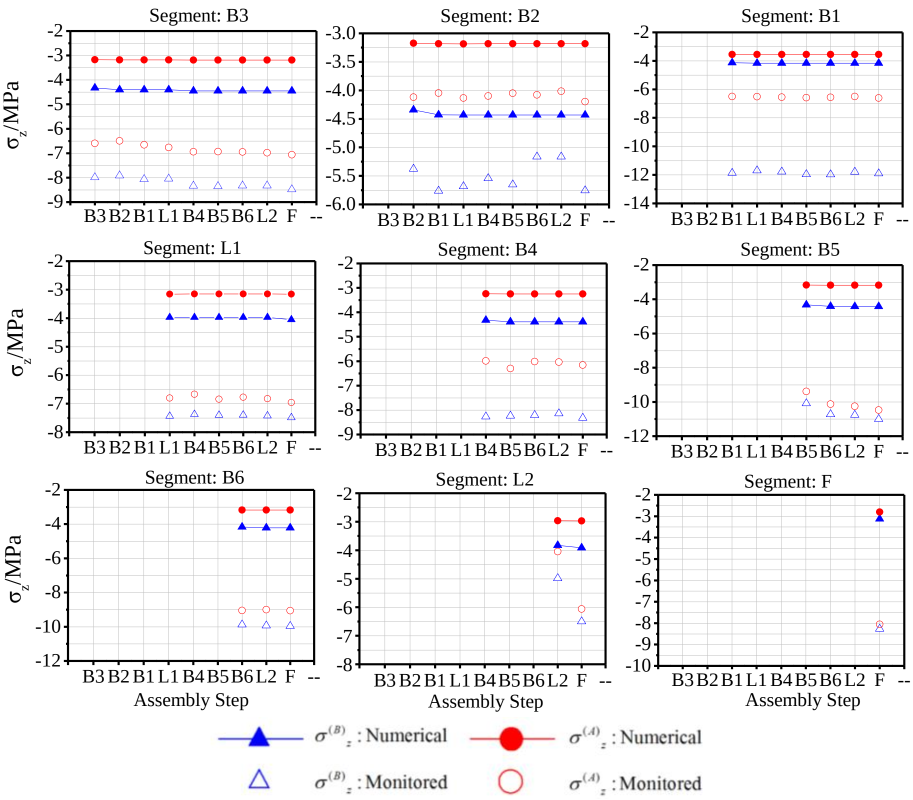

Fig. 14 Time history curves of the longitudinal stress in assembly stage

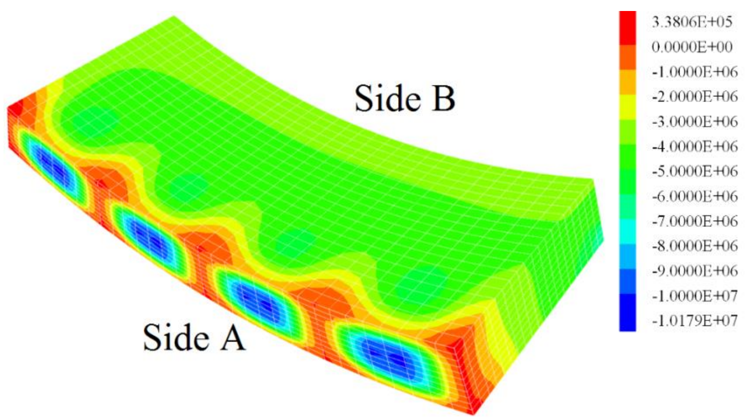

Fig. 15 The distribution of longitudinal stress after segments assembling (Unit: Pa)

Figs. 17 and 18 indicate that maximum principal tensile stress appears on segment's side surface and intrados in the middle of two adjacent jacks. In addition, the maximum tensile stress increases first and then tends to be stable before the insertion of key segment, however it decreases obviously in the step of key segment insertion. The maximum value of the maximum principal stress during the assembly stage is 0.752 MPa while the minimum value is 0.371 MPa. With the segments assembly processing, the stress concentration phenomenon appears gradually in the RC segment corners away from the jacks, which resulting in great principal tensile stress occurred and the maximum value of the principal tensile stress at segment corner rises to 0.35 MPa. The greater the principal tensile stress is, the easier the segment cracking occurred. In other word, it is indicated that segment's side surface and intrados in the middle of two adjacent jacks are the crack-sensitive position in the early assembly stage, and subsequently segment corners far away from the jacks become the crack-sensitive position either. The sensitive positions in the numerical results coincide with the in-situ investigation, which reveals that the large local principal tensile stress is the main reason causing the segment cracks during assembling. The concrete grade of Foguan Shiziyang tunnel is C50, and its design value of tensile strength is about 1.89 MPa (China Architecture and Building Press 2015). Although the

(a) Case 1 and Case 2

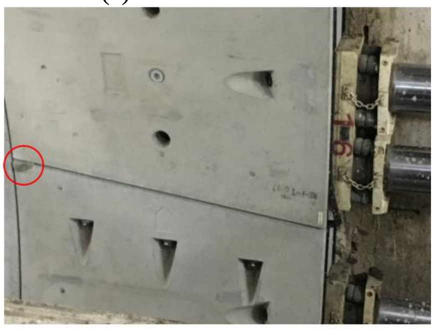

(b) Case 3

Fig. 16 The investigated cracks in assembly stage

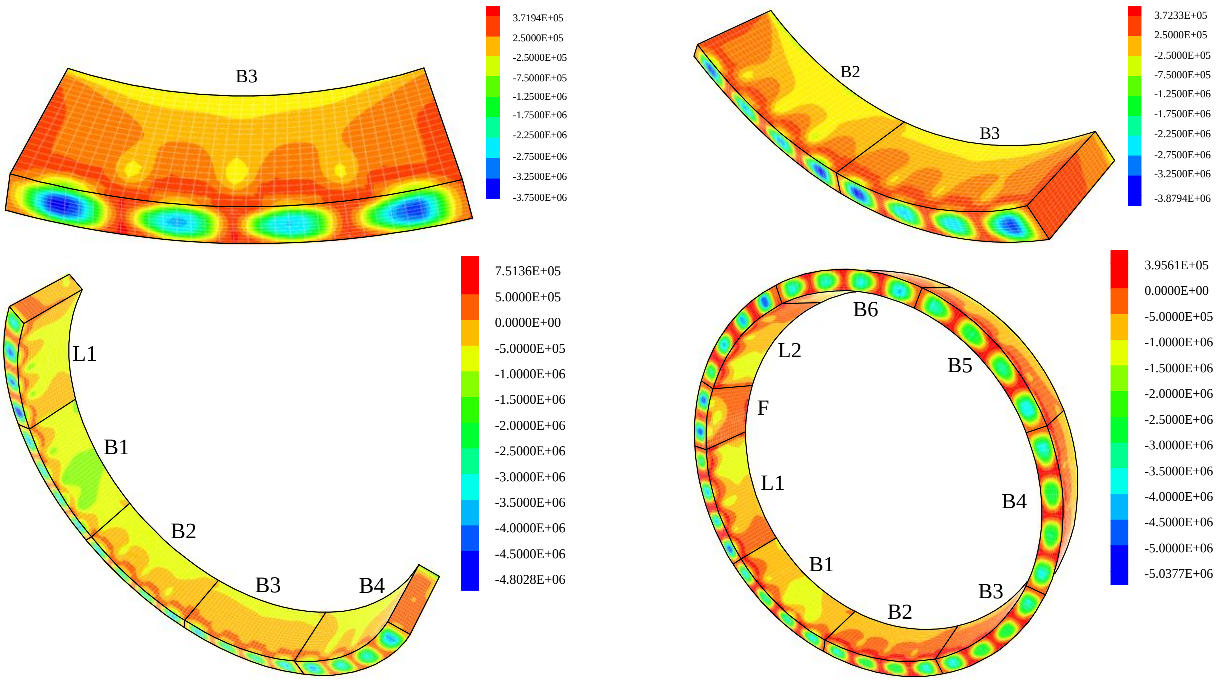

Fig. 17 Principal tensile stress of segments in assembly stage (Unit: Pa)

maximum principal tensile stress during assembling in the numerical results only accounts for 19.6%~39.8% of the tensile strength, the crack-sensitive positions will be easily damaged practically due to the misalignment stress caused by the factors such as assembly error, contact deficiencies, stiffness difference at the corner of sealing gaskets, etc., which makes the principal tensile stress in actual situation become larger than the calculation ones.

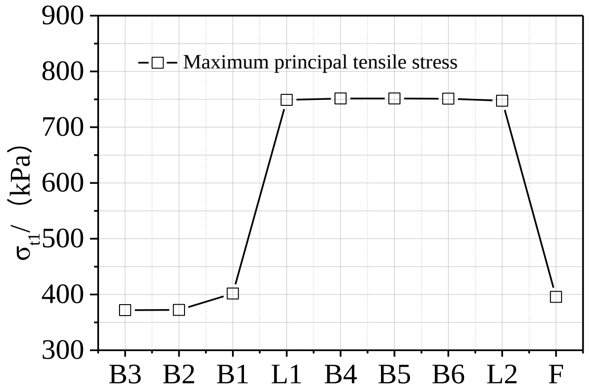

Fig. 18 Time history of maximum principal tensile stress in assembly stage

5. Discussion

The FDM model aiming at the simulation for the assembly process of Foguan Shiziyang shield tunnel doesn't take into account the unmanageable and stochastic factors including assembly error, pre-tightening force of bolts, contact deficiencies, stiffness difference at the corner of sealing gaskets, real-time adjustment of jack thrust and so on. Actually, however, those factors are rather common during tunneling, which causes significant assembly stress and local concentration phenomenon on assembling segments, and hence it will lead to that the monitored value of segment internal force become relative larger than that of numerical calculation.

According to the comparison analysis on the monitored value and the calculated value of mechanical response during assembling, those factors only have effects on the value of segment internal force and the adjustment of local stress, while it is barely influenced on the overall spatial distribution of internal forces and stress in the assembly stage. Thus, it can be drawn that the main loads of the assembling segmental ring are the jack thrust, the segment self-weight and the interaction among the segments.

During design and construction stages, necessary measures should be taken to prevent the crack-sensitive positions of the segments from damaging during assembling. The following suggestions are put forward based on this paper: first of all, the segment manufacturing should be strictly controlled to meet the design requirements on segment size and quality; secondly, the assembling technology of the construction crew should be improved to reduce and avoid the assembly error; in addition, there should be some local reinforcement on crack-sensitive positions and the sealing gaskets with soften corners should be adopted instead of the conventional type; the last but not least, jack thrust should be strictly controlled since excessive thrust will cause larger longitudinal stresses in adjacent side surface of segments and hence results in larger axial force and bending moment during the assembly stage.

6. Conclusions

The temporal-spatial distribution of axial force and bending moment as well as strain and stress of the assembling segmental ring were investigated and analyzed in depth by means of FDM numerical simulation and in-situ tests to ascertain the mechanical response of segments during the assembly stage. The conclusions can be drawn as below:

(1) The effects on axial force and bending moment caused by the assembly of adjacent segment are the most significant, followed by the insertion of the key segment, while the effects of the other assembly steps are relative smaller. Furthermore, the closer the monitored section to the adjacent segment or key segment, the more significant the inner forces response, and the insertion effects of key segment acquired by in-situ tests are more obvious than the numerical calculation.

(2) The calculated values of axial force are all in compression, while the monitored values are about 1.5~1.75 times larger than the calculated values. Simultaneously, the axial forces during assembling are about 9.7%~33.9% of those in normal service stage.

(3) The monitored values are two times larger than the calculated values. And the maximum values of the monitored positive bending moment and negative bending moment during assembling are about 59.4% and 39.3% of those in the normal service stage respectively. Furthermore, the bending moment is more sensitive to the segments assembly process compared with axial force, and it will result in the large bending moment of segments during assembling when the construction parameters are not suitable or the assembly error is too large, which should be concerned in large cross-section shield tunnel assembling.

(4) The assembling of the adjacent segments and the insertion of key segment will result in the increment longitudinal stress, and the disturbance is greater than the other assembly steps which shows the same changing of axial force and bending moment. It is indicated that the spatial distribution of the longitudinal stress is the original factor causing the changing of inner forces during assembling. Besides, there are local longitudinal tensile stress zones on segments side surfaces in the middle of two adjacent jacks at the side surfaces close to the jacks.

(5) The maximum principal tensile stress appears at the segment side surface and intrados in the middle of two adjacent jacks. Moreover, with the segments assembly processing, the stress concentration phenomenon occurs gradually at the RC segment corners away from the jacks, which results in larger principal tensile stress at the segment corner.

(6) The segment side surfaces and intrados in the middle of two adjacent jacks are the crack-sensitive positions in the early assembly stage and subsequently segment corners away from the jacks become the crack-sensitive positions either. The sensitive positions in the numerical results coincide with the in-situ investigation, which reveals that the larger local principal tensile stress is the main reason causing the segment cracking during assembling.

Acknowledgments

The authors appreciate the support of the National Key Research and Development Program of China (Grant No.2016YFC0802202) and the National Natural Science Foundation of China (Grant No.U1361210, No.51578462, No.51578459).

References

Blom, C.B.M., Van der Horst, E.J. and Jovanovic, P.S.（1999), “Three-dimensional structural analyses of the shield-driven “Green Heart” tunnel of the high-speed line south”, *Tunn. Undergr. Sp. Tech.*, **14**(2), 217-224.

Cavalaro, S.H.P., Blom, C.B.M., Aguado, A., et al. (2012), “New design method for the production tolerances of concrete tunnel segments”, *J. Perform. Constr. Fac*., **26**, 824-834.

Cavalaro, S.H.P., Blom, C.B.M., Walraven, J.C., et al. (2011), “Structural analysis of contact deficiencies in segmented lining”, *Tunn. Undergr. Sp. Tech*., **26**(6), 734-749.

Chen, J.S. and Mo, H.H. (2009), “Numerical study on crack problems in segments of shield tunnel using finite element method”, *Tunn. Undergr. Sp. Tech.*, **24**, 91-102.

Chen, J.S., Mo, H.H. and Liang Z.Y. (2006), “Study on local cracking of segments in shield tunnel during construction”, *Chinese J. Rock Mech. Eng.*, (5), 906-910. (in Chinese)

Feng, K., He, C., Fang, Y., et al. (2013), “Study on the mechanical behavior of lining structure for underwater shield tunnel of high-speed railway”, *Adv. Struct. Eng*., **16**(8), 1381-1399.

Feng, K., He, C., Qiu, Y., et al. (2018), “Full-scale tests on bending behavior of segmental joints for large underwater shield tunnels”, *Tunn. Undergr. Sp. Tech*., **75**, 100-116.

Guo, R., He, C., Su, Z.X., et al. (2011), “Study of shearing mechanical properties of segment joints of shield tunnels”, *Modern Tunn. Technol*., **48**(4), 72-77. (in Chinese)

Ishimura, K., Mashimo, H. and Ishimura, T. (2003), “How to evaluate the section force at the time of assembling of the segment”, *Study Tunnel Eng*., **13**(1), 395-400.

Itasca Consulting Group (2005), 'Fast Lagrangian Analysis of Continua in 3 Dimensions', Minneapolis: Itasca Consulting Group.

Liao, S.M., Men, Y.Q., Zhang, D., et al. (2014), “In-situ tests on mechanical behaviors during assembly of segmental linings of Qianjiang tunnel”, *Chinese J. Geotech. Eng*., **37**(1), 156-164. (in Chinese)

Liao, S.M., Xu, J. and Jiao Q.Z. (2013), “Mechanical behaviors of tunnel lining during segment assembly”, *China Civil Eng. J*., **46**(3), 127-135. (in Chinese)

Mo, H.H. and Chen, J.S. (2008), “Study on internal force and dislocation of segments caused by shield machine attitude”, *Tunn. Undergr. Sp. Tech.*, **23**, 281-291.

Oliveira, E.R.DE, A. and Chen, Y.T. (1985), “The difference and similarity between finite element and finite difference”, *China Water Sci. Technol. Inform.*, (4), 91-98. (in Chinese)

Sugimoto, M. (2006), “Causes of shield segment damages during construction”, International Symposium on Underground Excavation and Tunnelling. Bangkok, Thailand.

The Professional Standards Compilation Group of People's Republic of China, (2015), TB10003-2005 Code for Design of Concrete Structures, Beijing: China Architecture& Building Press. (in Chinese)

Wu, H.M., Shu, Y.M. and Zhu, J.G. (2011), “Implementation and verification of interface constitutive model in FLAC3D”, *Water Sci. Eng.*, **4**(3), 305-316.

Wu, M.Q. (2004), “Study on the application of steel fiber reinforced concrete shield tube in Subway Tunnel Engineering”, *Guangdong Build. Mater*., (3), 6-8. (in Chinese)

Xu, J. (2013), “Mechanical behaviors of tunnel linning induced by segments assembly”, Shanghai: Tongji University. (in Chinese)

Ye X.W., Ni Y.Q., Wai T.T., et al., 2013, 'A vision-based system for dynamic displacement measurement of long-span bridges: algorithm and verification', *Smart Struct. Syst*., **12**(3-4), 363-379.

Ye, X.W., Xi, P.S., Su, Y.H., et al. (2018), “Stochastic characterization of wind field characteristics of an arch bridge instrumented with structural health monitoring system”, *Struct. Saf*., **71**, 47-56.

Zhao W.S., Chen W.Z., Yang F. (2015), 'Study of the interface mechanical properties of concrete segments in shield tunnels', *Modern Tunnel. Technol*., **52**(3), 119-126. (in Chinese)